Electrically Active and Inactive B Lattice Sites in Ultrahighly B Doped Si(001): An X-Ray Near-Edge Absorption Fine-Structure and High-Resolution Diffraction Study

A. Vailionis, G. Glass, P. Desjardins, David G. Cahill, and J. E. Greene

Department of Materials Science, the Coordinated Science Laboratory and the Materials Research Laboratory, University of Illinois, 1101 West Springfield, Urbana, Illinois 61801

(Received 2 February 1999)

B lattice positions are determined as a function of B concentration C_B in ultrahighly doped Si(001):B layers grown by gas-source molecular beam epitaxy from B_2H_6/Si_2H_6. For $C_B \leq 2.5 \times 10^{20}$ cm^{-3}, all B atoms reside on tetrahedrally bonded electrically active substitutional Si sites. At higher C_B, inactive B is incorporated as B pairs located on single Si sites and oriented primarily along in-plane [100] and [010] directions. The B pairs are sp^2 bonded with trigonal coordination while substitutional single B atoms are sp^3. A surface reaction path leading to inactive B incorporation is proposed. [S0031-9007(99)09265-0]

PACS numbers: 61.72.Tt, 61.10.Ht, 68.55.Ln, 81.15.Gh

Si films with B concentrations far exceeding bulk solubility limits are of particular interest for nanoscale electronic device fabrication such as base layers in high frequency Si and $Si/Si_{1-x}Ge_x$ heterostructure bipolar transistors [1]. Although high dopant concentrations can be achieved by ion implantation, spreading of B profiles due to transient-enhanced diffusion during post annealing limits the formation of shallow abrupt junctions at submicron scales [2]. Gas-source molecular beam epitaxy (GS-MBE) offers the possibility of achieving ultrahigh doping concentrations, transport properties equivalent to bulk Si, and the formation of abrupt doping profiles *in situ* without subsequent annealing [3,4].

While the ability to prepare kinetically controlled ultrahigh B doped Si film structures represents an important advance, there is still little understanding of the reaction path leading to the incorporation of B in nonelectrically active sites during GS-MBE growth of Si(001):B with B concentrations $C_B > 2.5 \times 10^{20}$ cm^{-3}. For other common p- and n-type dopants such as Al, Ga, P, and Sb, the electrically active fraction progressively decreases as the dopant concentration is increased above the kinetic solubility limit [5]. This is due to the formation of precipitates which, once nucleated, act as sinks for dopant atoms and thus decrease the doping concentration in substitutional Si sites [6]. The second-phase precipitates typically exceed 10 nm in size and can therefore be detected by transmission electron microscopy (TEM). In the case of ultrahigh B doping, however, there are no credible reports of observed precipitates in as-grown layers suggesting that, if they are present, they must be in the form of small ($\lesssim$50 atoms) dispersed clusters. Moreover, unlike other dopants, the concentration N_B of electrically active B in GS-MBE Si(001) continues to increase with increasing C_B even as N_B/C_B decreases [3].

It has been suggested that B clustering is the cause of incomplete B activation in ion-implanted Si [7]. However, there has been no clear explanation of either the reaction path leading to inactive B incorporation or the site and local bonding configuration into which the inactive B is incorporated during film growth. A study of B ion-implanted depth distributions measured by secondary-ion mass spectrometry (SIMS) predicts that B clusters larger than five atoms are unstable [2]. B-Si interactions in small clusters have been modeled using *ab initio* methods based on density functional theory and the local density approximation [8,9]. The lowest-energy configuration for B clusters was proposed to be B pairs aligned along ⟨001⟩ directions and occupying single Si lattice sites.

The possible existence of small B clusters is difficult to test experimentally due to their weak scattering power. In the present study, carried out using ultrahigh B doped Si(001) layers grown by GS-MBE, we have used near-edge x-ray absorption fine-structure spectroscopy (NEXAFS) which has been shown to be capable of distinguishing sp^2 from sp^3 bonding in inorganic B-containing compounds [10,11]. In BF_3, hexagonal BN, and B_2O_3, where B is bonded to three atoms in a planar trigonal configuration, the $2p$ orbitals are split resulting in π (originating from $2p_z$ atomic orbitals) and σ (arising from hybridized $2s$, $2p_x$, and $2p_y$ atomic orbitals) molecular orbitals [12]. As a consequence, B in sp^2 coordination yields a sharp intense low-energy NEXAFS peak corresponding to a $1s \rightarrow 2p_z$ (π^*) excitation and a broad high-energy feature corresponding to the $1s \rightarrow \sigma^*$ transition. In contrast, for tetrahedrally sp^3 bonded B (e.g., in KBF_4 and cubic BN), all three hybridized p states are degenerate giving rise to only σ bonds. Therefore, NEXAFS spectra from sp^3 coordinated B compounds exhibit a single broad feature originating from overlapping $1s \rightarrow \sigma^*$ transitions [10,11].

In this Letter, we present the first experimental evidence, obtained using NEXAFS, high-resolution x-ray diffraction (HR-XRD), Hall-effect, and SIMS measurements for the incorporation of B pairs into substitutional Si sites. This occurs during GS-MBE growth when C_B exceeds 2.5×10^{20} cm^{-3}. The B pairs are electrically inactive as shown by temperature-dependent Hall measurements.

 0031-9007/99/82(22)/4464(4)$15.00 © 1999 The American Physical Society

Si(001):B layers with C_B ranging from 5×10^{16} to 1.2×10^{22} cm^{-3} were grown in ultrahigh vacuum (UHV) by GS-MBE using Si_2H_6 and B_2H_6 at temperatures $T_s =$ 600 °C, well above the monohydride desorption temperature [4]. Detailed information concerning film growth can be found elsewhere [4]. Film structural quality was examined by reflection high-energy electron diffraction, TEM, and HR-XRD. Si(001):B out-of-plane lattice parameters $a_\perp$ were obtained from HR-XRD ω-2θ measurements using a high-resolution diffractometer with a four-crystal Ge(220) monochromator and Cu $K_{\alpha 1}$ radiation ($\lambda = 1.540597$ Å). In-plane lattice constants $a_\parallel$ and residual strains were determined from high-resolution reciprocal lattice maps (HR-RLM) around asymmetric reflections. For these measurements, an additional two-crystal Ge(220) analyzer was placed in front of the detector and a series of ω-2θ scans was acquired at different ω offsets.

Total B concentrations C_B in as-deposited Si(001):B layers were determined by SIMS. Quantification, with an experimental uncertainty of 10%, was carried out by a comparison to B ion-implanted bulk Si(001) standards. Electrically active B concentrations N_B were obtained from temperature-dependent Hall-effect measurements in the van der Pauw configuration. For degenerate samples, we used the formalism of Bennett [13], based upon the earlier work of Klauder [14], to account for many-body interactions leading to changes in the density of states and narrowing of the band gap and to correct for the overestimate in N_B values provided by Hall measurements.

NEXAFS spectra, using both the total electron yield (TEY) and the fluorescence yield (FY) detection techniques, were acquired near the B 188-eV K-edge at the Canadian Grasshopper beam line of the Synchrotron Radiation Center in Stoughton, Wisconsin [15]. TEY is more surface sensitive, while FY is essentially a bulk probe.

All Si(001):B films were found to be epitaxial and completely coherent with the substrate as determined from HR-RLM. The inset in Fig. 1 shows a typical map around the asymmetric 113 reflection from a Si(001):B layer with $C_B = 4.2 \times 10^{21}$ cm^{-3} and $N_B = 7.8 \times 10^{20}$ cm^{-3}. Diffracted intensity distributions are plotted as isointensity contours as a function of the reciprocal lattice vectors $k_\parallel$ and $k_\perp$ parallel and perpendicular to the surface, respectively. The substrate and the film peaks are nearly perfectly aligned along the $k_\parallel$ direction indicating negligible in-plane strain relaxation. TEM results show no evidence of extended defects in the film.

Figure 1 is a plot of the out-of-plane lattice parameter $a_\perp$ as a function of C_B in Si(001):B films. For films with $C_B \leq 2.5 \times 10^{20}$ cm^{-3}, $a_\perp$ decreases linearly with increasing C_B. However, $a_\perp$ vs C_B becomes nonlinear for $C_B > 2.5 \times 10^{20}$ cm^{-3}. The initial linear $a_\perp(C_B)$ relationship is consistent with Vegard's rule as well as Hall measurements showing that all B is incorporated into electrically active substitutional sites (Table I). The data can be fit with the expression

$$a_\perp = a_{Si} - \beta N_B, \tag{1}$$

for which a_{Si} is the bulk Si parameter (5.431 Å), N_B is the active B acceptor concentration, and $\beta = 4.5 \times 10^{-23}$ Å cm^3 is the strain rate coefficient. Note that $\beta = [(1+\nu)/(1-\nu)][(a_{Si} - a_B)/n_{Si}]$, for which $\nu = 0.278$ is the Poisson ratio, $n_{Si} = 5 \times 10^{22}$ cm^{-3} is the atomic density of Si, and $a_B = 4.1$ Å is the lattice constant of diamond structure B calculated using the tetrahedral covalent radius, 0.88 Å.

As C_B is increased above 2.5×10^{20} cm^{-3}, $a_\perp$ continues to decrease but $a_\perp(C_B)$ becomes nonlinear as B is incorporated into both electrically active and inactive sites (Table I) in parallel reaction paths. A comparison of the $a_\perp(C_B)$ relationship for C_B less than and greater

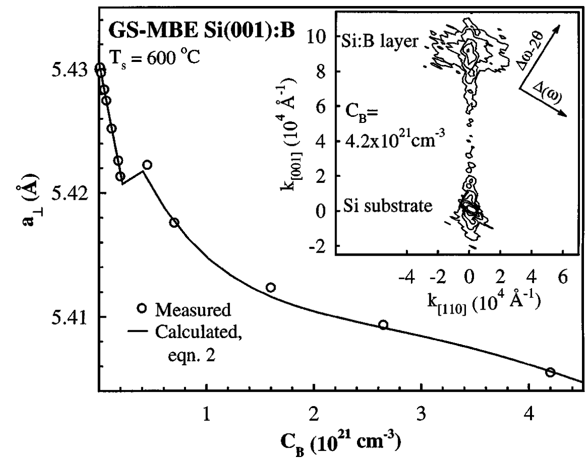

FIG. 1. Si(001):B lattice parameter $a_\perp$ along the film growth direction as a function of the total incorporated B concentration C_B. The inset shows a HR-RLM around the 113 reflection of a Si(001):B film with $C_B = 4.2 \times 10^{21}$ cm^{-3} and $N_B = 7.8 \times 10^{20}$ cm^{-3}.

TABLE I. Total (C_B), electrically active (N_B), and inactive B concentrations in B doped Si(001) layers.

Total B Concentration C_B (cm^{-3})	Active B Concentration N_B (cm^{-3})	Inactive B Concentration ($C_B - N_B$) (cm^{-3})
5.0×10^{18}	5.0×10^{18}	⋯
1.7×10^{20}	1.7×10^{20}	⋯
2.5×10^{20}	2.5×10^{20}	⋯
4.5×10^{20}	2.3×10^{20}	2.2×10^{20}
5.0×10^{20}	2.5×10^{20}	2.5×10^{20}
7.0×10^{20}	3.0×10^{20}	4.0×10^{20}
1.6×10^{21}	4.8×10^{20}	1.1×10^{21}
2.7×10^{21}	6.5×10^{20}	2.1×10^{21}
4.2×10^{21}	7.8×10^{20}	3.4×10^{21}
6.0×10^{21}	9.0×10^{20}	5.1×10^{21}
1.0×10^{22}	1.2×10^{21}	8.8×10^{21}
1.2×10^{22}	1.3×10^{21}	1.1×10^{22}

than 2.5×10^{20} cm^{-3} shows that while the incorporation of electrically active B results in purely in-plane tensile strain, the presence of B in the electrically inactive configuration gives rise to compressive strain. The full set of $a_\perp$ vs C_B data, including the kink in the curve as (C_B-N_B) becomes larger than zero, is well described (see Fig. 1) by the addition of another term to Eq. (1) to yield

$$a_\perp = a_{Si} - \beta N_B + \alpha(C_B - N_B). \quad (2)$$

α, the inactive-B strain coefficient, is 4.8×10^{-24} Å cm^3. The fact that the entire curve can be fit with a single value of α suggests that all inactive B is incorporated into a single type of configuration, whose size remains constant, in the Si lattice irrespective of C_B.

Typical B K-edge TEY and FY NEXAFS spectra, obtained with the x-ray beam incident at 20° to the sample normal, are shown in Fig. 2 for films with C_B values between 5×10^{18} and 1×10^{22} cm^{-3}. The 196 eV peak, corresponding to the B $1s \rightarrow 2p_z$ (π^*) transition, is present for all films, but is much more pronounced in the surface sensitive TEY spectra. The broad feature at 205 eV, due to the B $1s \rightarrow \sigma^*$ transition, is clearly visible in the TEY spectra. We assign both peaks to B_2O_3 formed at the surface due to a combination of B segregation during film growth [4] and subsequent sample air exposure.

The NEXAFS peak located at 192 eV emerges in the layer with $C_B = 5 \times 10^{20}$ cm^{-3}, and the intensity of the peak increases sharply with further increase in C_B. This peak is much more prominent in the FY than in the TEY

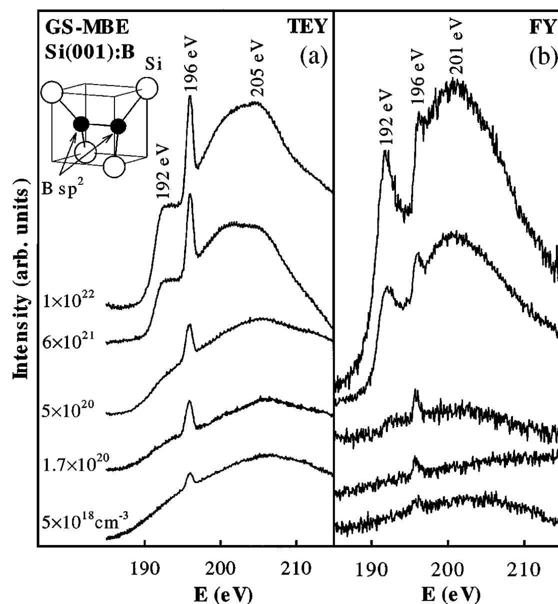

FIG. 2. (a) Total electron yield (TEY) and (b) fluorescence yield (FY) NEXAFS spectra obtained near the B K-edge of GS-MBE Si(001):B layers with C_B ranging from 5.0×10^{18} to 1.0×10^{22} cm^{-3}. The inset shows a B pair incorporated into electrically inactive sp^2 bonded trigonally coordinated substitutional sites in a Si tetrahedron.

NEXAFS spectra. Since the effective electron escape depth for semiconductors with incident x-ray radiation in the 100–200 eV range is <100 Å compared to a fluorescence photon escape depth of >1000 Å [15], the peak at 192 eV must be related to bulk rather than surface B.

The 192 eV feature in Fig. 2 cannot be attributed to previously reported B-related species with similar peak positions: o-carborane ($B_{10}H_{10}C_2H_2$), diborane (B_2H_6), and decaborane ($B_{10}H_{14}$) [16]. SIMS measurements show that C in our films is below the detection limit, 5×10^{16} cm^{-3}, while boron hydrides either dissociatively chemisorb or desorb from short-lived physisorbed states at the film growth temperatures employed. We attribute the 192 eV peak to a B $1s \rightarrow 2p_z$ transition corresponding to sp^2 bonded B incorporated as B pairs located at single Si sites (inset of Fig. 2). In this configuration, each B is surrounded by three atoms: two Si and one B, and has a planar trigonal coordination. The fact that this peak is at a lower energy than the sharp peak arising from surface B_2O_3 is consistent with the lower Pauling electronegativity values of Si (1.8) and B (2.0) compared to O (3.5).

The broad feature in FY spectra near 201 eV (also visible, although weaker, in the surface-sensitive TEY spectra) is attributed to a convolution of contributions arising from B $1s \rightarrow \sigma^*$ transitions associated with sp^2 B-B and B-Si (B in the electrically inactive configuration) bonds together with sp^3 B-Si (B in the electrically active configuration) bonds. The individual peaks cannot be resolved.

Angle-dependent NEXAFS measurements were carried out on the Si(001):B layer with $C_B = 1.0 \times 10^{22}$ cm^{-3}, for which the electrically inactive B concentration (C_B-N_B) $= 8.8 \times 10^{21}$ cm^{-3} (Table I), in order to determine the polarization dependence of the B $1s \rightarrow 2p_z$ (π^*) signal. The angle θ between the film surface normal and the direction of the incident beam was varied between 10° and 60°. If all B pairs were oriented along the [001] growth direction, i.e., π^* orbitals oriented along $[hk0]$ with $h, k = \pm 1$, the intensity I of the 192 eV feature should be proportional to $\cos^2\theta$. However, if the B pairs are in plane with π^* orbitals aligned along $[0kl]$ and $[h0l]$ with k, l and $h, l = \pm 1$, I should be independent of θ. We did not observe a strong dependence of I on θ indicating that most of the B pairs are oriented in plane. Within the resolution of the measurements, we cannot, however, rule out the possibility that the B pairs are randomly oriented, with $\frac{1}{3}$ of them along [001], which would give only a weak $I(\theta)$ dependence.

Based upon the above results, we propose the following reaction paths for B incorporation in ultrahighly doped GS-MBE Si(001):B layers. During Si(001):B film growth at $C_B \leq 2.5 \times 10^{20}$ cm^{-3}, C_B increases linearly with the B_2H_6/Si_2H_6 flux ratio and incorporated B segregates to the second layer [4] with a coverage $\theta_B \leq \theta_{B,sat} =$ 0.5 ML (monolayer), the saturation value [4,17]. All B

incorporated in these layers is located at tetrahedrally coordinated substitutional Si sites and is electrically active. As a result, $a_\perp$ for these films decreases linearly with increasing C_B and the 192 eV NEXAFS peak is absent.

When C_B exceeds 2.5×10^{20} cm^{-3}, the B incorporation rate increases (i.e., C_B increases with B_2H_6/Si_2H_6 flux ratio at a faster rate), $\theta_B > \theta_{B,sat}$ during film growth, and, as has been recently shown by isotopically tagged temperature-programmed desorption, B begins to accumulate at the outer surface [4]. B surface adatoms are mobile at the growth temperatures employed and form B pairs which are then incorporated as a unit into the growing Si film. Simultaneous with the overall increase in the B incorporation rate, the fraction of electrically active B decreases from unity (Table I). This is consistent with the B pairs being incorporated with trigonal symmetry on substitutional Si sites such that all B σ-bonds are saturated. Furthermore, incorporation of electrically inactive B at the expense of active B decreases the overall tensile strain in the layer by contributing a compressive component (Fig. 1).

Previous *ab initio* calculations show that the lowest-energy configuration for B pairs in Si is for the bond direction to be along ⟨100⟩ with a B-B bond length $r_{\text{B-B}} = 1.6 \pm 0.2$ Å [8,9]. Using this result with our angle-resolved NEXAFS data which rule out the possibility that the B-B bonds are all aligned along the [001] growth direction, we calculated, based upon the value of α obtained from Fig. 1 and Eq. (2), the bond length between a nearest-neighbor Si and a B pair atom for two cases: (1) all B pairs are aligned in-plane equally along [100] and [010] directions, and (2) the pairs are distributed randomly in all three orthogonal directions. The results yield $r_{\text{Si-B}_{\text{pair}}} = 2.18$ and 2.01 ± 0.04 Å, respectively. $r_{\text{Si-B}_{\text{pair}}}$ for case (2) agrees with total energy calculations predicting a value of 2.01 Å for randomly aligned ⟨100⟩ B pairs [8].

In summary, we have shown that B in GS-MBE Si(001):B layers grown from B_2H_6/Si_2H_6 mixtures is incorporated into electrically active sp^3 bonded tetrahedral sites at concentrations N_B up to 2.5×10^{20} cm^{-3}. For layers with higher B concentrations ($C_B = 5 \times 10^{20}$–1.2×10^{22} cm^{-3}), N_B continues to increase with increasing C_B, but the electrically active B fraction N_B/C_B decreases rapidly. Electrically inactive B is incorporated as sp^2 bonded trigonally coordinated B pairs in substitutional Si sites giving rise to a strong $1s \rightarrow 2p_z$ (π^*) NEXAFS feature. We propose a surface reaction path leading to B dimer incorporation which is consistent with our HR-XRD measurements. That is, when the second-layer B coverage during film growth exceeds the saturation value of 0.5 ML (corresponding to $C_B = 2.5 \times 10^{20}$ cm^{-3}), excess B accumulates at the outer surface where it forms stable B pairs which are incorporated as a unit in substitutional sites, thus reducing the overall in-plane tensile strain.

The authors gratefully acknowledge the financial support of the Semiconductor Research Corporation and the U.S. Department of Energy, Division of Materials Sciences (Award No. DEFG02-ER9645439). P. D. is partially supported by NSERC (Canada). They also thank Dr. K. Tan and Dr. M. Kasrai for the help with the NEXAFS experiments.

[1] Z. Matutinovickrstelj, V. Venkataraman, E.J. Prinz, J.C. Sturm, and C.W. Magee, IEEE Trans. Electron Devices **43**, 457 (1996).
[2] P.A. Stolk, H.-J. Gossmann, D.J. Eaglesham, and J.M. Poate, Nucl. Instrum. Methods Phys. Res., Sect. B **96**, 187 (1995).
[3] G. Glass, H. Kim, P. Desjardins, N. Taylor, T. Spila, Q. Lu, and J.E. Greene (unpublished).
[4] H. Kim, G. Glass, T. Spila, N. Taylor, S.Y. Park, J.R. Abelson, and J.E. Greene, J. Appl. Phys. **82**, 2288 (1997); G. Glass, H. Kim, M.R. Sardela, Q. Lu, J.R.A. Carlsson, J.R. Abelson, and J.E. Greene, Surf. Sci. **392**, L63 (1997).
[5] Reported equilibrium solid solubilities at 900 °C are 6×10^{20} cm^{-3} for P, 3×10^{19} cm^{-3} for Sb, 2×10^{19} cm^{-3} for Ga, and 1.5×10^{19} cm^{-3} for Al. For B in Si, reported solid solubilities range from 2×10^{19} cm^{-3} at 700 °C to 8×10^{20} cm^{-3} at 1400 °C. See *Impurities and Defects in Group IV Elements and III-V Compounds,* edited by O. Madelung and M. Schulz, Landolt-Börnstein, New Series, Group III, Vol. 22, Pt. a (Springer-Verlag, Berlin, 1989).
[6] P. Ostoja, D. Nobili, A. Armigliato, and R. Angelucci, J. Electrochem. Soc. **123**, 124 (1976).
[7] F.N. Schwettmann, J. Appl. Phys. **45**, 1918 (1974).
[8] E. Tarnow, J. Phys. Condens. Matter **4**, 5405 (1992).
[9] J. Zhu, T. Diaz de la Rubia, L.H. Yang, C. Mailhiot, and G.H. Gilmer, Phys. Rev. B **54**, 4741 (1996).
[10] W.H.E. Schwarz, L. Mensching, K.H. Hallmeier, and R. Szargan, Chem. Phys. **82**, 57 (1983).
[11] L.J. Terminello, A. Chaiken, D.A. Lapiano-Smith, D.L. Doll, and T. Sato, J. Vac. Sci. Technol. A **12**, 2462 (1994).
[12] See, for example, J. Stöhr, *NEXAFS Spectroscopy,* Springer Series in Surface Science Vol. 25 (Springer, New York, 1996), and references therein.
[13] H.S. Bennett, J. Appl. Phys. **59**, 2837 (1986).
[14] J.R. Klauder, Ann. Phys. **14**, 43 (1961).
[15] M. Kasrai, Z. Yin, G.M. Bancroft, and K.H. Tan, J. Vac. Sci. Technol. A **11**, 2694 (1993).
[16] M.W. Ruckman, M.F. Murray, J.K. Mowlem, and D.R. Strongin, J. Vac. Sci. Technol. A **11**, 2477 (1993).
[17] Y. Wang, R.J. Hamers, and E. Kaxiras, Phys. Rev. Lett. **74**, 403 (1995).